# Unveiling the thermo-structural setting of collisional orogens

## *Example from the Variscan chain in Sardinia*

**Alessandro Petroccia**
Dipartimento di Scienze della Terra, Università di Torino, Via Valperga Caluso 35, 10125, Torino, Italia
DOI:10.19276/plinius.2023.01.010

## INTRODUCTION

The geodynamic evolution of collisional orogens has been classically described using an orogenic wedge model, in which different rock packages experience different finite tectono-metamorphic histories (e.g., Jaquet et al., 2018). The hinterland-foreland transition zone is characterized by the progressive transition from tectonic units occurring in the metamorphic core of the belt to the ones deformed at shallower crustal levels and steadily included in the orogenic wedge (Thigpen et al., 2010, 2017).

Different features control the thermo-structural architecture and variation across orogenic wedges, such as the efficiency of erosion, the temperature/deformation ratio within nappes and the presence of ductile tectonic contacts (Jamieson et al., 2002).

Despite the relevance of this topic and the widespread distribution within orogenic wedges, relatively few methods are available for low-grade metapelites (Frey, 1987; Frey & Robinson, 1999). Thus, the unravelling of the thermo-structural architecture of this sector of the belt is hampered by the presence of strongly deformed large-scale nappes made by apparently homogeneous low-grade metasedimentary rocks lacking index minerals useful for pressure and temperature (*P-T)* estimations. In addition, the presence of strong overprinting belonging to the post-nappe stacking deformation that modifies the original attitude of pre- and syn-nappe stacking elements complicates the untangling of this area.

The Variscan belt in Sardinia represents a continental crustal section, exposing a quite continuous metamorphic field gradient from greenschist- to granulite-facies rocks (Carmignani et al., 1994; Cruciani et al., 2015 for a review). This work aimed to reconstruct the thermo-structural architecture of the low-grade Internal and External Nappe Zone exposed in the hinterland-foreland transition zone in Sardinia and of the ductile boundary in between (i.e., the Barbagia Thrust). In order to explore these topics, an approach with a broad perspective was chosen, combining fieldwork with different scales of structural analysis, and quantitative temperature constraints by RSCM, coupled with kinematics of the flow and finite strain estimations.

## GEOLOGICAL SETTING

The Sardinian Variscan belt comprises: (i) the External Zone, (ii) the Axial Zone, and (iii) the Nappe Zone (Fig. 1a; Carmignani et al., 1994). The latter has been divided into External (central to southern Sardinia) and Internal (northern to central Sardinia) Nappe Zone. The boundary between them is marked by a regional-scale, top-to-the S-SW thrust-sense ductile to brittle shear zone, the Barbagia Thrust (BT; Fig. 1a,b,c; Carosi & Malfatti, 1995; Montomoli et al., 2018; Petroccia et al., 2022a,b). The Internal Nappe Zone (Fig. 1a) includes the Low-Grade Metamorphic Complex (LGMC), which reached low- to upper-greenschist-facies metamorphic conditions, and the Medium-Grade Metamorphic Complex (MGMC), which reached amphibolite-facies conditions (Franceschelli et al., 1989; Carosi et al., 2020, 2022; see Cruciani et al., 2015 for a review). In the External Nappe Zone, all units are characterized by syn-tectonic regional greenschist-facies metamorphism (Carosi et al., 1991, 2004, 2010; Franceschelli et al., 1992; Petroccia et al., 2022a,b,c), except for the deepest Monte Grighini Unit, which reached amphibolite-facies conditions (Musumeci, 1992; Cruciani et al., 2016). The investigated area comprehends both the Barbagia Unit (BU) and the Meana Sardo Unit (MSU), belonging to the Internal and External nappes, and the northernmost sector of the Low-Grade Metamorphic Complex, belonging to the Internal Nappe Zone, close to Lula and Bitti towns (Fig. 1b,c).

## METHODOLOGY

### Vorticity and finite strain analysis

The non-coaxiality of the flow in shear zones is defined by the $W_k$ number (Xypolias, 2010), which several vorticity analysis techniques can estimate. Pure and simple shear components may be described through the di-

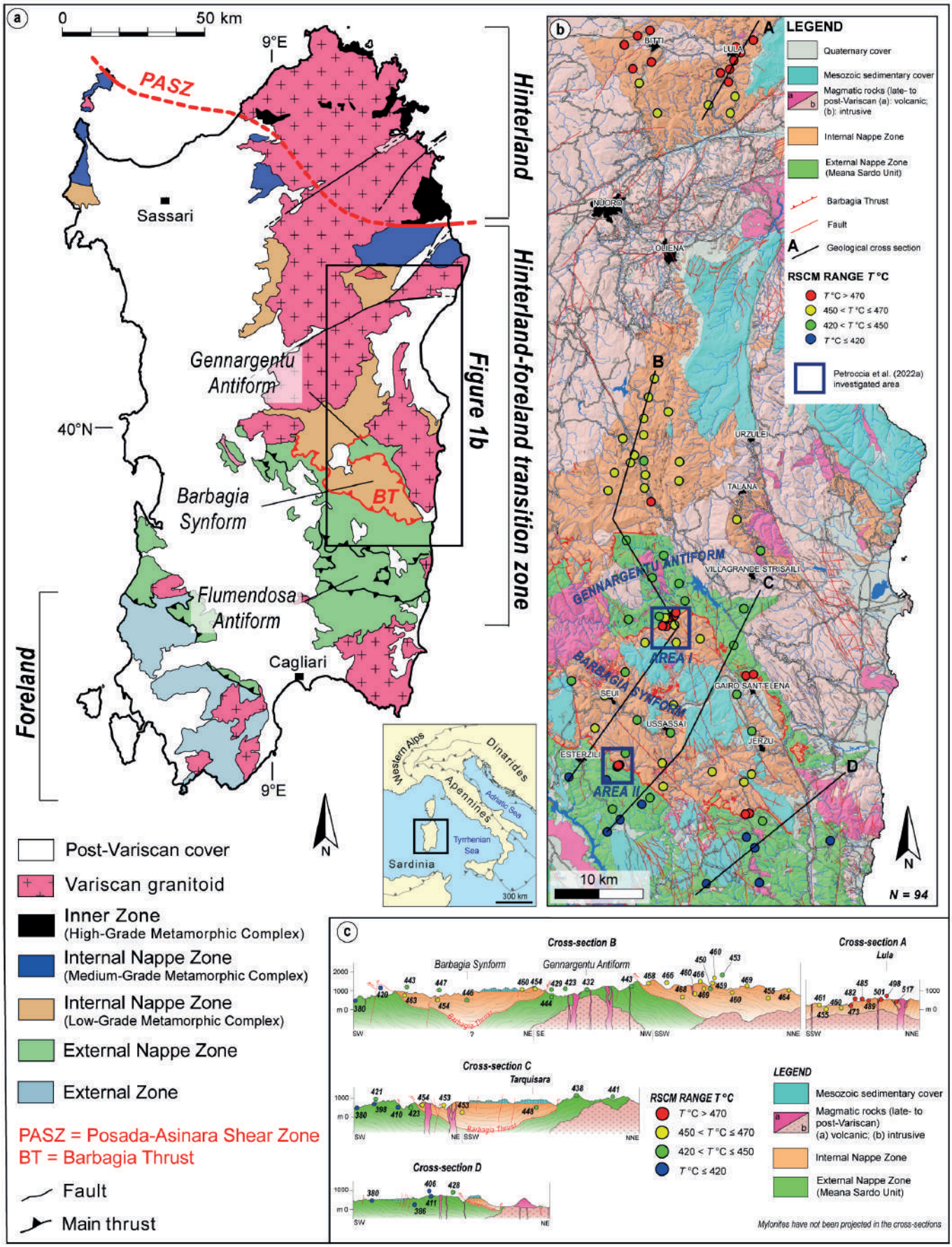


***Figure 1 a)*** *Geographic position and tectonic sketch map of the Sardinia island (modified from Carmignani* et al.*, 1994; Petroccia* et al.*, 2022c). Location of Figure 1b is highlighted by a black rectangle;* ***b)*** *Schematic geological map of the investigated area showing Tmax distribution and the trace of the cross-sections presented in Figure 1c. The location of the areas investigated by Petroccia* et al.*, 2022a is displayed by the blue rectangles;* ***c)*** *Data plotted on the geological cross sections compiled after Carmignani* et al. *(1994), and the 1:50.000 geological maps of Jerzu and Muravera (CARG project). Symbols for Tmax refer to samples projected on the cross-section topography.*

mensionless $W_m$. The mean kinematic vorticity number ($W_m$) could be assumed to be equal to $W_k$ because it represents the average value over the deformation interval during which the structure or fabric formed (Xypolias, 2010). Pure and simple shear is associated with $W_k = 0$ and $W_k = 1$, respectively.

In the present work, the C' shear band method (Kurz & Northrup, 2008; Gillam et al., 2013) and two different porphyroclasts-based methods, the porphyroclast aspect ratio method (PAR; Passchier, 1987; Wallis et al., 1993) and the rigid grain net method (RGN; Jessup et al., 2007), have been applied to evaluate the percentage of pure and simple shear of the BT. The nominal error for vorticity analysis is ± 0.1 (Tikoff & Fossen, 1995). A comparison of different possible systematic error sources indicates that for medium to low vorticity numbers ($W_m$ < 0.8), the vorticity data minimum systematic error is ± 0.2 (Iacopini et al., 2011).

Finite strain analyses were performed using the centre-to-centre method (Fry, 1979) by the EllipseFit 3.8.0 software (Vollmer, 2015). Samples were cut and polished perpendicular to the foliation and both parallel and perpendicular to the mineral lineation (XZ and YZ sections of finite strain ellipsoid). This method is based on the redistribution of the centres of the strain markers caused by deformation and is independent from their shape. Data have been plotted on the Flinn diagram.

### Raman Spectroscopy on Carbonaceous Material (RSCM) geothermometer

The peak temperature was derived using Raman Spectroscopy on Carbonaceous Material (RSCM) geothermometer. This method is based on the progressive transformation of Carbonaceous Material (CM) during the temperature increase, and it is not affected by the retrograde history (i.e., the $T_{max}$; Beyssac *et* al., 2002). The Raman spectrum of perfect graphite is made by a single G band and other two bands D1 and D2. The intensity of the D1 band is used to evaluate the degree of disorder in the CM. Beyssac et al. (2002) established a correlation between the temperature and Raman parameters of the CM called R2. The RSCM geothermometer has an absolute precision of ± 50°C due to uncertainties of the petrological data used for the calibration. The relative uncertainties on temperature are ± 10-15°C if the guidelines and recommendations of Beyssac et al. (2002, 2004) and Lündsorf et al. (2014, 2017) are followed. Raman microspectroscopy has been performed with the Horiba Jobin Yvon LabRam HRVIS Raman System at the Centro "G. Scansetti", Dipartimento di Scienze della Terra, Università degli Studi di Torino. Before each measurement session, the spectrometer was calibrated using the 520.5 $cm^{-1}$ peak (r band) of a silicon standard. Spectra were acquired by a beam spot of approximately one μm diameter with a green Nd 532.06 nm laser source at 80 mW, corresponding to 2-4 mW at the sample surface, with a 100x magnification. For each sample, a minimum of 10 spectra was recorded, except for samples containing very little CM amount. The peak position, band area, and bandwidth (FWHM) were determined using the computer program PeakFit 4.0, following the fitting procedure described by Beyssac et al. (2002). The fitting itself followed the Voigt area, and the algorithm combined Gaussian and Lorentzian profiles. Because obtained spectra were acquired using a green Nd 532.06 nm laser, the RSCM temperature estimates discussed in the following sections were derived from the Aoya et al. (2010) calibration, which was established based on the same laser wavelength.

## STRUCTURAL AND RSCM RESULTS

### Internal and External nappes

Detailed mapping, coupled with multi-scale structural observations, allowed the definition of a polyphase evolution (see Petroccia et al., 2022a,b for further explanation and the mapped area), consisting of three ductile deformation phases developed under a contractional tectonic regime ($D_1$-$D_2$-$D_3$) and the fourth one under extensional conditions ($D_4$). The prominent deformation phase ($D_2$) is responsible for the development of the main foliation ($S_2$). It becomes more mylonitic moving toward the BT and displays several kinematic indicators with a main top-to-the S-SW sense of shear. The $S_2$ foliation is marked by greenschist-facies mineral assemblage. $D_1$ and $D_2$ structural elements are widely deformed by weakly asymmetric to upright $F_3$ folds. Folds with sub-horizontal axial planes ($F_4$), developed during the orogenic extensional phase ($D_4$), are recognizable.

In the northernmost investigated sector of the Internal Nappe Zone (Fig. 2), the derived $T_{max}$ within the Lula and Bitti villages agree with those obtained with thermodynamic modelling estimations (~450-470°C) on nearby samples by Costamagna et al. (2012), highlighting the reliability of the obtained RSCM results. The presence of garnet, plagioclase, biotite and white mica in the northernmost rocks is in agreement with the obtained $T_{max}$ of ~500-520°C and *P-T* data from Franceschelli et al. (1989).

The central Nappe Zone, where the BU juxtaposed onto the MSU crops out, is characterized by a more complex thermal architecture driven by regional scale antiform and synform (see Fig. 1a and Fig. 2). The BU displays a general $T_{max}$ of ~470-440°C whereas the MSU has $T_{max}$ of ~440-380°C (Fig. 2). Previous investigations do not document a thermal difference between the BU and MSU (Franceschelli et al., 1992; Carosi et al., 2010; Montomoli et al., 2018). However, the $T_{max}$ coverage highlights a systematic difference of ~10-20°C between them within the Gennargentu Antiform and ~30-70°C in the southernmost sector (Fig. 1b, c and Fig. 2). The $T_{max}$ shifting between the MSU and the BU is higher in the southernmost sector (~30-70°C) than within the Gennargentu Antiform (~10-20°C). The post-nappe stacking folded structure is also highlighted by the presence of the BT with the same structural and kinematic features and high $T_{max}$ in the two limbs of the Barbagia Synform

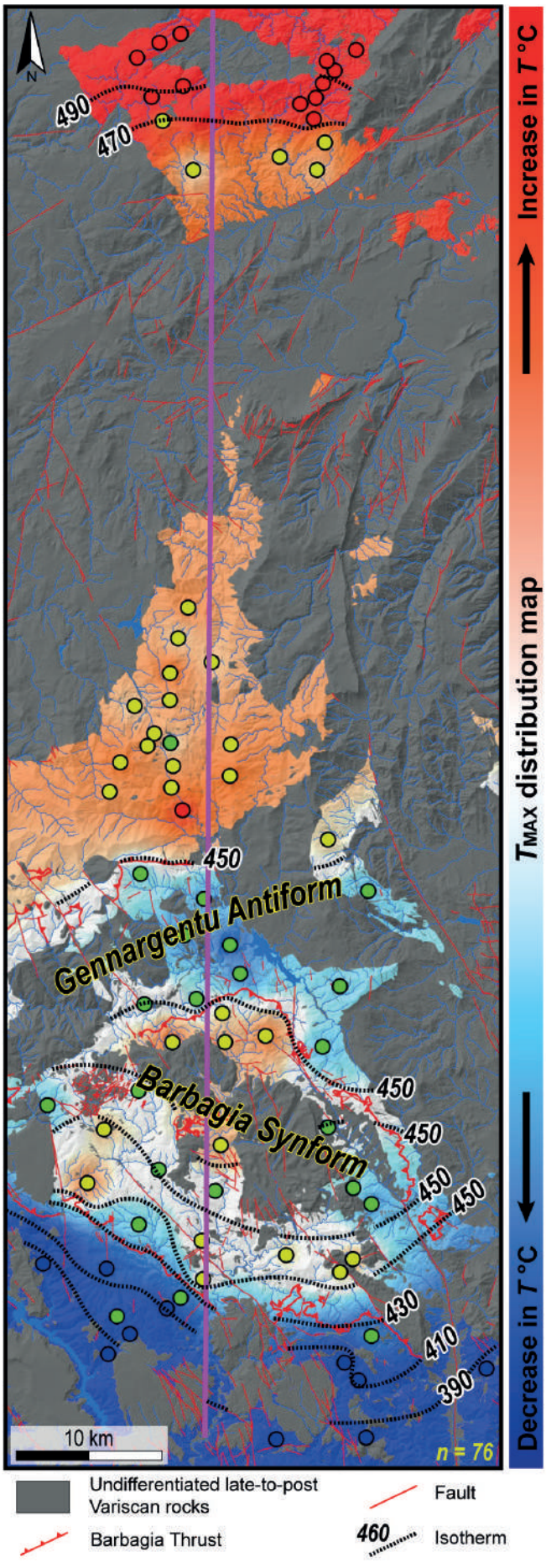


***Figure 2*** *Tmax contour map and isotherms of the investigated area from Petroccia et al., 2022c. See Figure 1c for the symbology of RSCM data. The trace of the simplified tectonic cross-section shown in Figure 5a has been displayed in purple.*

(see Petroccia et al., 2022a).

## Barbagia Thrust

Detailed meso- and microstructural analyses have been performed in two different sectors of the BT in the Sardinian Variscan belt (Fig. 1b). This region has undergone a polyphase evolution consisting of four ductile deformation phases (see the previous chapter and Petroccia et al., 2022a,b). The main structures of the study area are caused by the $D_2$ deformation phase. This phase is linked to the syn-nappe stacking and exhumation of the BU (Carosi et al., 2004; Montomoli et al., 2018). An increase in shear deformation along with the progressive transposition of previous $D_1$ structures approaching the BT has been highlighted, as shown in Fig. 3a,b. The $S_2$ foliation, parallel to the boundaries of the shear zone, and the $F_2$ fold axes, perpendicular to the $L_2$ object lineation, are coeval with the overthrust of the Internal Nappe Zone onto the External Nappe Zone (Carosi et al., 2004). The syn-kinematic mineral assemblage (chlorite + white mica) along the $S_2$ mylonitic foliation is indicative of greenschist-facies metamorphic conditions. This is, in agreement with the main dynamic recrystallization mechanism of quartz, indicative of temperature between 400 and 450°C (BLG II and local SGR; Stipp et al., 2002). Kinematic indicators, both at the meso- and microscale, reveal a top-to-the-S-SW sense of shear. This also agrees with the S-SW $F_2$ fold vergence detailed by previous authors (Carosi, 2004; Carosi et al., 2004; Montomoli et al., 2018). The whole architecture of the Nappe Zone is affected by regional-scale $F_3$ folds ($D_3$). The $D_3$ phase is characterized by pressure solution, indicating an upper structural level deformation. Also, the presence of the BT mylonitic zone in the different sectors of the Barbagia Synform, with the same structural and kinematic features, indicates that $F_3$ folding deformed this tectonic contact. Similar structural results and the same shear sense were obtained from both zones, confirming the post-nappe stacking folded structure (i.e., Barbagia Synform; Fig. 1b,c). Subsequent post-collision extensional tectonics was characterized by the development of open folds ($F_4$).

Montomoli et al. (2018) performed both illite and chlorite crystallinity measurements on samples transecting the BT but found no systematic changes in those parameters across the structural profile. $T_{max}$ across the BT on both strongly and weakly deformed samples have been measured from two different structural sectors of the same shear zone (Fig. 1b). An increase in temperature moving from the structurally higher parts of the BU, or from the structurally lower parts of the MSU, toward the BT core has been highlighted. The detected $T_{max}$ shift between non-mylonitic and mylonitic rocks is in the range of ~50-70°C (Fig. 3c). $T_{max}$ for non-mylonitic rocks range from ~420 to ~450°C, in agreement with the documented metamorphic mineral assemblage and recry-

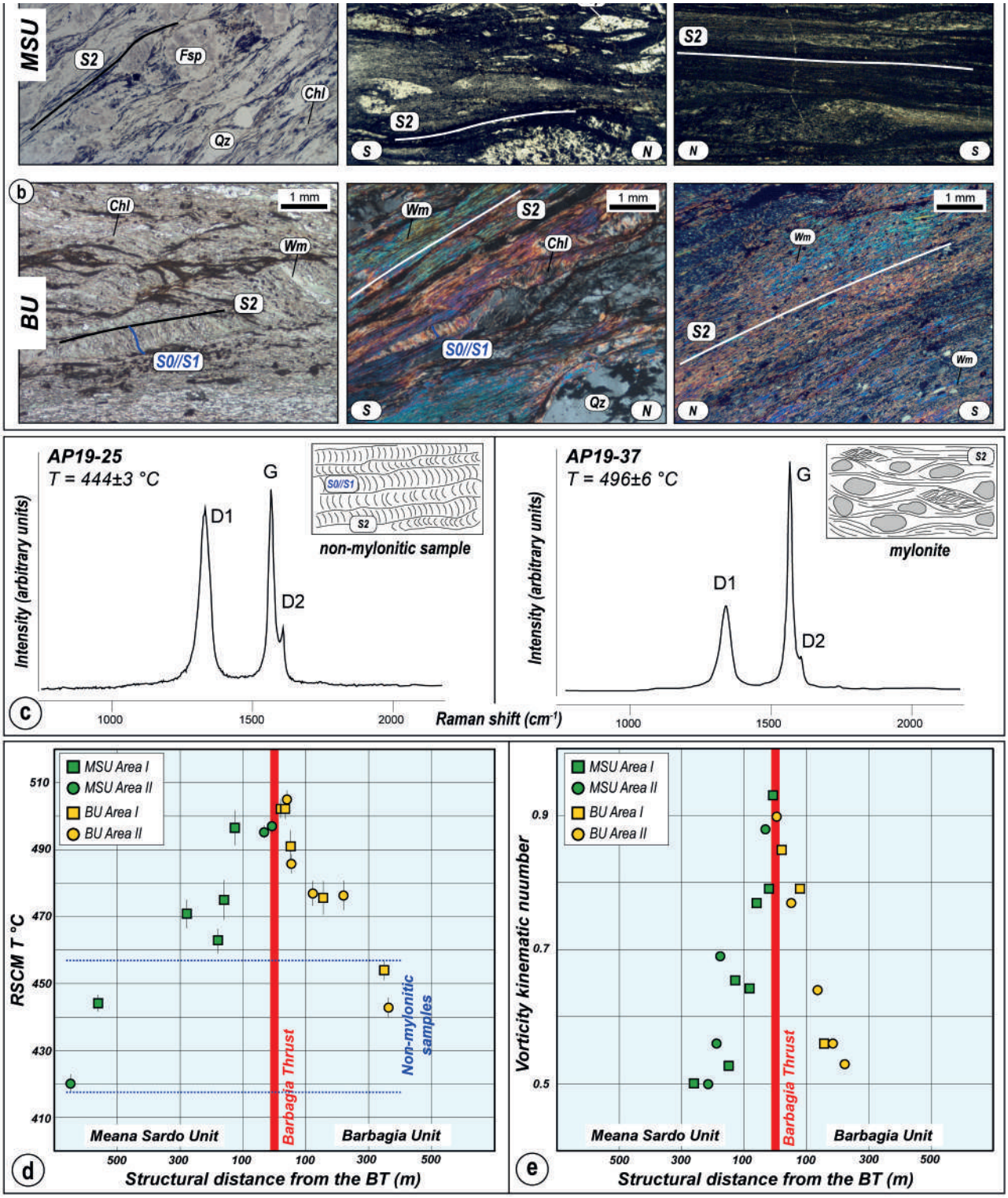


*Figure 3 a, b) Structural variation going toward the Barbagia Thrust in both units: a) variation from mylonites (on the left) to ultramylonites (on the right) in metavolcanic rocks belonging to the MSU; b) progressive variation of the foliation from spaced cleavage to a continuous cleavage moving toward the BT in metasedimentary rocks; **c)** Representative Raman spectra for CM from MSU samples AP19-25 and AP19-37, respectively outside and inside the mylonitic zone. Note that the Tmax is higher in the mylonite; **d)** Distribution of Tmax compared with the sample structural distance with respect to the BT; **e)** Distribution of estimated vorticity kinematic number against the structural distance from the BT*

stallization mechanism of quartz. In comparison, mylonites return higher $T_{max,}$ ranging from ~470 to ~500°C (Fig. 3c, d).

Several factors could cause this rise in temperature towards the core of shear zones: (i) graphite precipitation from a hydrothermal fluid; (ii) detrital graphite; (iii) strain reorganization of graphite; and (iv) shear heating. The $T_{max}$ reported here shows a persistent and systematic increase in $T_{max}$ with increasing strain intensity progressively moving into the BT high strain shear zone. All characteristics point to shear heating phenomena (see Petroccia et al., 2022a for a complete discussion).

The kinematic vorticity data obtained through the C' shear bands method (Kurz & Northrup, 2008), PAR, and the RGN method (Jessup et al., 2007) have allowed quantification of the flow regime as a non-coaxial flow. The obtained data highlight that the simple shear component increases progressively towards the centre of the

BT, from both MSU and BU rocks (Fig. 3e). A variation of simple shear from ~33% up to ~77% has been recognized. Mylonites and less deformed rocks record a flow regime dominated by pure shear, whereas ultramylonites in the center of the shear zone record an increasing amount of simple shear (Fig. 3e). This is associated with a change in the finite strain ellipsoid from close to the plane strain up to prolate conditions. A higher Rxz value is inferred from ultramylonitic samples only within the core of the shear zone. This implies that the core of the BT accommodated a higher amount of strain compared to the shear zone peripheries (Fossen & Cavalcante, 2017). Higher $W_k$ values within the centre of the BT, and a prolate strain ellipsoid are associated with higher $T_{max}$, whereas lower $W_k$ values, far from the BT core, and plane strain conditions are associated with samples showing lower $T_{max}$ (Fig. 3d, e).

The progressive increase in temperature towards the BT, coupled with the increase of simple shear, could indicate a syn-shearing temperature imprint (Petroccia et al., 2022a). This broad correlation between $T_{max}$ and the deformation gradient could imply that the flow path was combined with by a progressive localization of deformation in the core of the shear zone, due to thermal weakening, during the ductile deformation.

## DISCUSSION AND CONCLUSION

A polyphase deformation history regarded as the result of pre-, syn- to post-nappe stacking evolution developed under contractional ($D_1$ to $D_3$) and extensional conditions ($D_4$), has been recognized. Also, RSCM data provide quantitative $T_{max}$ constraints at the belt scale with a relative uncertainty of less than 10-15°C. This highlights a complex thermal orogenic wedge architecture previously unrecognized (Petroccia et al., 2022a,c). Deforming the primary bedding $S_0$, far from the main tectonic contacts, the $D_1$ event is well-recognizable, both at micro- and mesoscale, in the hinge of the $D_2$ folds and in $S_2$ microlithons (Fig. 4). This event has been associated with the burial and the pre-nappe stacking during the early collisional stage and the orogenic wedge growth (Carmignani et al., 1994; Carosi et al., 2004; Conti et al., 1999, 2001; Montomoli et al., 2018). The $D_2$ deformation phase at the belt scale is linked to the syn-collisional exhumation associated with the Barbagia Thrust (BT) shear activity (Montomoli et al., 2018 and references therein). The $D_2$ is associated with both folding and shearing with a top-to-S-SW vergence and sense of shear, respectively (Fig. 4). The presence of the BT mylonitic zone in the different sectors of the Barbagia Synform, with the same structural and kinematic features and the same $T_{max}$ distribution, emphasizes the presence of regional-scale antiforms and synforms, driving the present-day thermo-structural architecture of the belt (Fig. 5a,b). All these results are in agreement with the model

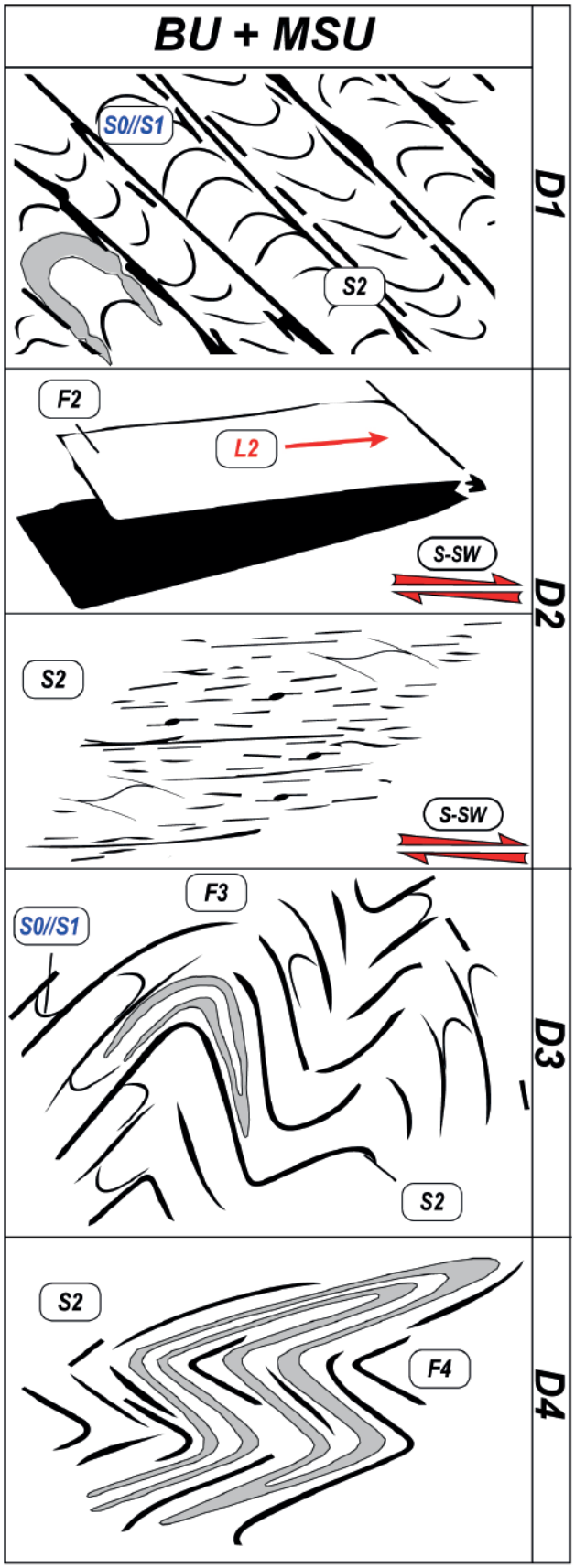


***Figure 4*** *Synoptic reconstruction of the field and microstructural investigations of the deformation history of the BU and MSU.*

of Carmignani et al. (1994) and Conti et al. (1999), which highlighted the presence of large-scale structures acquired in a contractional setting during the late deformation stage of crustal thickening and not during the late orogenic extension. Subsequent post-collision and post-nappe-stacking or transpression were characterized by

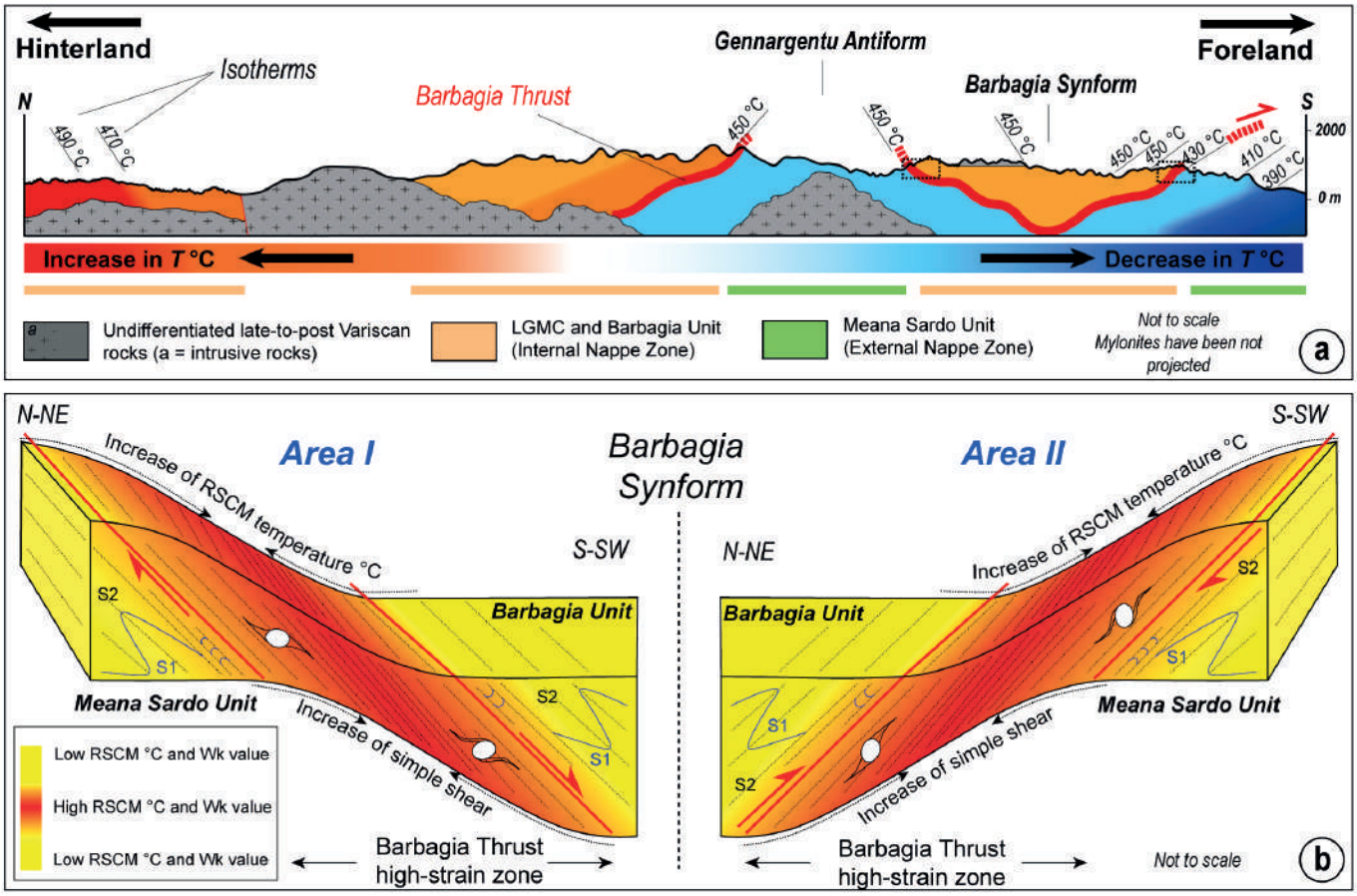


*Figure 5 a) Thermal architecture of the study area in a cross-section view (see Fig. 2 for the trace of the cross-section). Orange and green bars refer to the spatial extension of the Internal and External nappes respectively. The thick red line, that marks the BT, suggests the role of shear heating along the shear zone. The spatial distribution of the isotherms occurrence is displayed. The position of both Area I and Area II has been provided; b) Not to scale representations of the BT, along which the northern and southern limb of the Barbagia Synform, have been displayed. The progressive strain partitioning and gradient, from fold structures to a mylonitic foliation (approaching the Barbagia Thrust high-strain zone), have been highlighted, mirrored by the increase of both simple shear and the Tmax.*

the development of open folds with sub-horizontal axial plane and axes ($D_4$; Fig. 4).

Obtained results support a scenario of (Fig. 5a,b): (i) early collision and $T_{max}$ acquisition, different between Internal and External nappes ($D_1$; Fig. 5a); (ii) syn-collisional exhumation of the Internal Nappe Zone associated with shear heating along thrust-sense structures (i.e., the BT; Fig. 5b) ($D_2$); (iii) subsequent regional-scale folding during the latest stage of collision, that drove the present-day $T_{max}$ architecture ($D_3$; Fig. 5a). A late extensional stage ($D_4$), with the development of collapse folds with associated brittle/ductile to brittle structures, marks the end of the orogenic cycle.

## REFERENCES


Aoya, M., Kouketsu, Y., Endo, S., Shimizu, H., Mizukami, T., Nakamura, D., & Wallis, S. (2010): Extending the applicability of the Raman carbonaceous-material geothermometer using data from contact metamorphic rocks. *J. Metamorph. Geol.*, **28(9)**, 895-914.

Beyssac, O., Bollinger, L., Avouac, J.P., & Goffé, B. (2004): Thermal metamorphism in the lesser Himalaya of Nepal determined from Raman spectroscopy of carbonaceous material. *EPSL*, **225(1-2)**, 233-241.

Beyssac, O., Goffé, B., Chopin, C., & Rouzaud, J.N. (2002): Raman spectra of carbonaceous material in metasediments: a new geothermometer. *J. Metamorph. Geol.*, **20(9)**, 859-871.

Carmignani, L., Carosi, R., Di Pisa, A., Gattiglio, M., Musumeci, G., Oggiano, G., & Pertusati, P.C. (1994): The hercynian chain in Sardinia (Italy). *Geodin. Acta*, **7(1)**, 31–47.

Carosi, R. (2004): Carta geologico-strutturale del Monte S. Vittoria (Sarcidano-Barbagia di Belvì, Sardegna centrale, Italia). Carosi R., Elter F.M. Gattiglio M. (1997). Scala 1:25.000, Centro Offset, Siena, 1997. *Atti Soc. Toscana Sci. Nat. Mem. A*, **108**.

Carosi, R., & Malfatti, G. (1995): Analisi Strutturale dell'Unità di Meana Sardo e caratteri della deformazione duttile nel Sarcidano-Barbagia di Seulo (Sardegna centrale, Italia). *Atti Soc. Toscana Sci. Nat. Mem. A*, **102**, 121-136.

Carosi, R., Iacopini, D., & Montomoli, C. (2004): Asymmetric folds development in the Variscan Nappe of central Sardinia (Italy). *CR. GEOSCI.*, **336(10)**, 939-949.

Carosi, R., Leoni, L., Paolucci, F., Pertusati, P.C., & Trumpy, E. (2010): Deformation and illite crystallinity in metapelitic rocks from the Mandas area, in the Nappe Zone of the Variscan belt of Sardinia. *Rend. Online Soc. Geol.*, **11**, 393-394.

Carosi, R., Montomoli, C., Iaccarino, S., Benetti, B., Petroccia, A., & Simonetti, M. (2022): Constraining the timing of evolution of shear zones in two collisional orogens: fusing structural geology and geochronology. *Geosc.,* **12**, 231.

Carosi, R., Musumeci, G., & Pertusati, P.C. (1991): Differences in the structural evolution of tectonic units in central-southern Sardinia. *Boll. Soc. Geol. Ital.,* **110(3-4)**, 543-551.

Carosi, R., Petroccia, A., Iaccarino, S., Simonetti, M., Langone, A., & Montomoli, C. (2020): Kinematics and timing constraints in a transpressive tectonic regime: the example of the Posada-Asinara shear zone (NE Sardinia, Italy). *Geosc.,* **10**, 288.

Conti, P., Carmignani, L., Cerbai, N., Eltrudis, A., Funedda, A., & Oggiano, G. (1999): From thickening to extension in the Variscan belt - kinematic evidence from Sardinia (Italy). *Terra Nova,* **11(2/3)**, 93-99.

Conti, P., Carmignani, L., & Funedda, A. (2001): Change of nappe transport direction during the Variscan collisional evolution of central-southern Sardinia (Italy). *Tectonophysics,* **332(1-2)**, 255-273.

Costamagna, L.G., Cruciani, G., Franceschelli, M., & Puxeddu, M. (2012): A volcano-sedimentary sequence with albitite layers in the Variscan basement of NE Sardinia: a petrographical and geochemical study. *Period. di Mineral.,* **81(2)**, 179-204.

Cruciani, G., Franceschelli, M., Massonne, H.-J., Musumeci, G., & Spano, M.E. (2016): Thermomechanical evolution of the highgrade core in the nappe zone of Variscan Sardinia, Italy: the role of shear deformation and granite emplacement. *J. Metamorph. Geol.,* **34**, 321-342.

Cruciani, G., Montomoli, C., Carosi, R., Franceschelli, M., & Puxeddu, M. (2015): Continental collision from two perspectives: a review of Variscan metamorphism and deformation in northern Sardinia. *Period. di Mineral.,* **84**, 657-699.

Fossen, H., & Cavalcante, G.C.G. (2017): Shear zones–A review. *Earth. Sci. Rev.,* **171**, 434-455.

Franceschelli, M., Gattiglio, M., Pannuti, F., & Fadda, S. (1992): Illite crystallinity in pelitic rocks from the external and nappe zones of the Hercynian chain of Sardinia. In L., Carmignani, F.P., Sassi (Ed.). *Contributions to the Geology of Italy with special regard to the Paleozoic Basements*. (pp. 127–135) IGCP Project No. **276**, Newsletter.

Franceschelli, M., Memmi, I., Pannuti, F., & Ricci, C.A. (1989): Diachronous metamorphic equilibria in the Hercynian basement of northern Sardinia, Italy. *Geol. Soc. Spec. Publ.,* **43(1)**, 371-375.

Frey, M. (1987): Very low grade metamorphism of clastic sedimentary rock. In M., Frey (Ed.). *Low temperature metamorphism*. Chapman and Hall, New York, pp 9-57

Frey, M., & Robinson, D. (1999): Low-grade metamorphism. Blackwell Science, Oxford. pp. 312

Fry, N. (1979): Random point distribution and strain measurement in rocks. *Tectonophysics*, **60**, 89-105.

Gillam, B.G., Little, T.A., Smith, E., & Toy, V.G. (2013): Extensional shear band development on the outer margin of the Alpine mylonite zone, Tatare Stream, Southern Alps, New Zealand. *J. Struct. Geol.,* **54**, 1-20.

Iacopini, D., Frassi, C., Carosi, R., & Montomoli, C. (2011): Biases in three-dimensional vorticity analysis using porphyroclast system: limits and application to natural examples. *Geol. Soc. Spec. Publ.,* **360(1)**, 301-318.

Jamieson, R.A., Beaumont, C., Nguyen, M.H., Lee, B. (2002): Interaction of metamorphism, deformation and exhumation in large convergent orogens. *J. Metamorph. Geol.,* **20(1)**, 9-24.

Jaquet, Y., Duretz, T., Grujic, D., Masson, H., & Schmalholz, S.M. (2018): Formation of orogenic wedges and crustal shear zones by thermal softening, associated topographic evolution and application to natural orogens. *Tectonophysics,* **746**, 512-529.

Jessup, M.J., Law, R.J., & Frassi, C. (2007): The Rigid Grain Net (RGN): An alternative method for estimating mean kinematic vorticity number (Wm). *J. Struct. Geol.,* **29**, 411–421.

Kurz, G.A., & Northrup, C.J. (2008): Structural analysis of mylonitic rocks in the Cougar Creek Complex, Oregon–Idaho using the porphyroclast hyperbolic distribution method, and potential use of SC′-type extensional shear bands as quantitative vorticity indicators. *J. Struct. Geol.,* **30(8)**, 1005-1012.

Lünsdorf, N.K., Dunkl, I., Schmidt, B.C., Rantitsch, G., & Von Eynatten, H. (2014): Towards a higher comparability of geothermometric data obtained by Raman spectroscopy of carbonaceous material. Part I: evaluation of biasing factors. *Geostand. Geoanal. Res.,* **38**, 73-94.

Lünsdorf, N.K., Dunkl, I., Schmidt, B.C., Rantitsch, G., & Von Eynatten, H. (2017): Towards a higher comparability of geothermometric data obtained by Raman spectroscopy of carbonaceous material. Part 2: A revised geothermometer. *Geostand. Geoanal. Res.,* **41(4)**, 593-612.

Montomoli, C., Iaccarino, S., Simonetti, M., Lezzerini, M., & Carosi, R. (2018): Structural setting, kinematics and metamorphism in a km-scale shear zone in the inner nappes of Sardinia (Italy). *Ital. J. Geosci.,* **137**, 294-310.

Musumeci, G. (1992): Ductile wrench tectonics and exhumation of hercynian metamorphic basement in Sardinia: Monte Grighini Complex. *Geodin. Acta,* **5(1-2)**, 119-133.

Passchier, C. W. (1987): Stable positions of rigid objects in non-coaxial flow–a study in vorticity analysis. *J. Struct. Geol.,* **9(5-6)**, 679-690.

Petroccia, A., Carosi, R., Montomoli, C., Iaccarino, S., & Vitale Brovarone, A. (2022a): Deformation and temperature variation along thrust-sense shear zones in the hinterland-foreland transition zone of collisional settings: a case study from the Barbagia Thrust (Sardinia, Italy). *J. Struct. Geol.,* **161**, 104640.

Petroccia, A., Montomoli, C., Iaccarino, S., & Carosi, R. (2022b): Geology of the contact area between the Internal and External Nappe Zone of the Sardinian Variscan Belt (Italy): new insights on the complex polyphase deformation occurring in the hinterland-foreland transition zone of collisional belts. *J. Maps,* **18(2)**, 472-483**.**

Petroccia, A., Carosi, R., Montomoli, C., Iaccarino, S., & Vitale Brovarone, A. (2022c): Thermal variation across collisional orogens: insights from the hinterland-foreland transition zone of the Sardinian Variscan belt. *Terra Nova,* **35(2)**, 113-123.

Stipp, M., Stünitz, H., Heilbron, M., & Schmid, D.W. (2002): The eastern tonale fault zone: A natural laboratory for crystal plastic deformation of quartz over a temperature range from 250 to 700°C. *J. Struct. Geol.,* **24**, 1861-1884.

Thigpen, J.R., Ashley, K.T., & Law, R.D. (2017): Evaluating kinematic displacement rate effects on transient thermal processes in thrust belts using coupled thermo-mechanical finite-element models. In R.D., Law, J.R., Thigpen, A.J., Merschat, & H.H. Stowell, (Ed.). *Linkage and Feedbacks in Orogenic Systems.* (213, pp. 1-23). *Mem. Geol. Soc. Am.*

Thigpen, J.R., Law, R.D., Lloyd, G.E., Brown, S.J., & Cook, B. (2010): Deformation Temperatures, Vorticity of Flow and Strain Symmetry in the Loch Eriboll Mylonites, NW Scotland: Implications for the Kinematic and Structural Evolution of the Northernmost Moine Thrust Zone. *Geol. Soc. Spec. Publ.,* **335**, 623-662.

Tikoff, B., & Fossen, H., (1995): The limitations of three-dimensional kinematic vorticity analysis. *J. Struct. Geol.,* **17**, 1771–1784.

Vollmer, FW. (2015): EllipseFit 3.2.

Wallis, S.R., Platt, J.P., & Knott, S.D. (1993): Recognition of synconvergence extension in accretionary wedges with examples from the Caiabrian Arc and the Eastern Alps. *Am. J. Sci.,* **293**, 463–495.

Xypolias, P. (2010): Vorticity analysis in shear zones: A review of methods and applications. *J. Struct. Geol.,* **32**, 2072–2092.